

# Measurement-induced chaos in an iterated Tavis-Cummings scheme

Juan Mauricio Torres, József Zsolt Bernád, and Gernot Alber  
*Institut für Angewandte Physik, Technische Universität Darmstadt, D-64289, Germany*

Orsolya Kálmán and Tamás Kiss  
*Institute for Solid State Physics and Optics, Wigner Research Centre,  
 Hungarian Academy of Sciences, P.O. Box 49, H-1525 Budapest, Hungary*  
 (Dated: October 3, 2016)

We propose a cavity QED scheme based on the Tavis-Cummings model to realize a conditional, non-linear dynamics exhibiting complex chaos in an ensemble of two-level atoms. The atoms interact pairwise with the coherent cavity field, which is subjected to homodyne measurement after the interaction. One member of the pair of atoms is then measured and upon condition that it is found in its ground state the other member of the pair is kept, otherwise discarded. The quantum state of the resulting ensemble of atoms is related to the state of the original ensemble via a non-linear transformation. By iterating this process with the help of an optical conveyor belt, for example, one arrives at complex deterministic chaos, where the evolution of pure quantum states is sensitive to the initial conditions. We uncover basic features of this dynamics by exploring stability regions in the space of initial states and analyze the occurrence of stable periodic orbits in dependence of the parameters of the model. It is demonstrated that sensitivity to initial conditions can be applied to amplify small differences of quantum states.

PACS numbers:

## I. INTRODUCTION

Strong sensitivity to initial conditions is a signature of chaotic behavior in dynamical systems [1]. In closed quantum systems, however, such a behavior is excluded by the linearity of the unitarity of the time evolution. Nevertheless, despite this characteristic linearity of closed quantum systems, chaotic features can arise in open quantum systems [2]. In particular, non-linear quantum state transformations can arise when identically prepared quantum systems are subjected to an entangling unitary transformation and a subsequent selective measurement performed on parts of the system [3]. Iterating such non-linear quantum state transformations may result in strong dependence on the initial conditions and in complex chaos [4].

Quantum state purification protocols involving identically prepared weakly entangled two-qubit systems, as introduced by Bennett and Deutsch [5, 6], are typical examples involving repeated sequences of unitary entangling transformations and selective conditional quantum measurements [7]. In these protocols the parameters are designed in such a way that quantum state purification can be achieved and a complicated dependence on initial conditions is avoided [8]. Nevertheless, it has been demonstrated that in general an intricate dependence of the resulting entanglement on the initially prepared states will occur [9]. Sensitivity to initial conditions can also be used for amplifying small initial differences of quantum states (Schrödinger microscope [10]). However, it has been demonstrated that such an amplification requires necessarily a large number of identically prepared systems which have to be discarded during the process [11].

Recent advances of quantum technology have enabled

the control of complicated many-body quantum systems to an unprecedented degree of accuracy so that even subtle effects of quantum measurement-induced nonlinearities may become amenable to experimental observation [12, 13]. In particular, the area of cavity quantum electrodynamics offers interesting perspectives for future experiments in these directions in view of its possibilities to measure and control the interaction of individual atoms with a single mode of the quantized radiation field with high precision [14, 15].

In this paper we explore the intricate nonlinear properties of measurement-induced chaos in a cavity quantum electrodynamical scenario. This scenario is a generalization of the dynamics of a one-atom-micro-maser [16] which may be viewed as an early example of an iterative unitary quantum dynamics conditioned on state selective quantum measurements. Motivated by recent experimental advances which realize the Tavis-Cummings model [15] we consider an ensemble of identically prepared two-level atoms (qubits) which interact pairwise with a single mode of the radiation field. Afterwards, one member of each pair and the corresponding cavity field are measured. Conditioned on the measurement results, the unmeasured atoms are kept or discarded. In practice, this may be implemented with the help of a single cavity and a pair of optical conveyor belts [14]. The atoms are moved through the cavity by the conveyor belts in such a way that only one pair of atoms interacts with the cavity mode at a time and then the cavity is re-initialized after each interaction. The remaining atoms form a new identically prepared ensemble of smaller size. Similar as in entanglement distillation protocols, the state changes of the remaining two-level atoms are described by an iterated nonlinear quantum transformation. It is demonstrated that this nonlinear quantum transformation ex-

hibits measurement-induced chaos and the resulting Julia sets can be connected or disconnected. Furthermore, it is demonstrated that this nonlinear quantum map can implement a Schrödinger microscope capable of amplifying the distinguishability of non-orthogonal quantum states.

The paper is organized as follows. In Sec. II we solve the dynamical equation of the two-atom Tavis-Cummings model. We present exact and approximate analytical solutions that facilitate the analysis of the dynamics. Furthermore, we briefly explain the atomic postselection scheme assisted by projection of the field. This is used in Sec. III to introduce a protocol that implements a nonlinear mapping of atomic probability amplitudes. In Sec. IV we analyze the fractal structure in the complex plane after iteration of the ideal map and compare with the numerical implementation using the exact-numerical quantum operation. In Sec. V we present a possible application, where the non-linear dynamics transforms two, initially close quantum states into almost orthogonal ones in a few steps of the protocol. Finally, in Sec. VI we propose a setup based on currently available experimental technology capable of implementing this few-step scenario.

## II. THE TWO-ATOM TAVIS-CUMMINGS MODEL

The two atoms Tavis-Cummings model describes the resonant interaction between two atoms, say  $A$  and  $B$ , and a single mode of the radiation field [17]. The atoms have ground states  $|0\rangle_i$  and excited states  $|1\rangle_i$  ( $i \in \{A, B\}$ ) separated by an energy difference of  $\hbar\omega$  which matches the energy of a photon inside the empty cavity. In the interaction picture the Hamiltonian can be expressed in the following form

$$\hat{H} = \hbar g \sum_{i=A,B} (\hat{\sigma}_i^+ \hat{a} + \hat{\sigma}_i^- \hat{a}^\dagger) \quad (1)$$

where  $\hat{\sigma}_i^+ = |1\rangle\langle 0|_i$  and  $\hat{\sigma}_i^- = |0\rangle\langle 1|_i$  are the atomic raising and lowering operators ( $i \in \{A, B\}$ ), and  $\hat{a}$  ( $\hat{a}^\dagger$ ) is the annihilation (creation) operator of the single mode field. The interaction picture is taken with respect to the reference Hamiltonian  $\hat{H}_0 = \omega(\hat{a}^\dagger \hat{a} + |1\rangle\langle 1|_A + |1\rangle\langle 1|_B)$  which is a constant of motion as it commutes with the interaction Hamiltonian  $\hat{H}$ . For this reason both operators,  $\hat{H}$  and  $\hat{H}_0$ , can be diagonalized simultaneously. In fact, there is a set of common eigenvectors with eigenvalue zero, namely  $\{|\Psi^-\rangle|n\rangle\}_{n=0}^\infty$ . These states are written in terms of the Fock states  $|n\rangle$  of the field and the atomic states  $|i, j\rangle = |i\rangle_A |j\rangle_B$  ( $i, j \in \{0, 1\}$ ) together with the atomic Bell states

$$|\Psi^\pm\rangle = \frac{1}{\sqrt{2}} (|0, 1\rangle \pm |1, 0\rangle). \quad (2)$$

The evaluation of the rest of the eigenvectors can be simplified by realizing that  $\hat{H}$  has a block-diagonal form in

the basis

$$\begin{aligned} &\{|0, 0\rangle|0\rangle\} \oplus \{|\Psi^+\rangle|0\rangle, |0, 0\rangle|1\rangle\} \oplus \\ &\{|1, 1\rangle|n-2\rangle, |\Psi^+\rangle|n-1\rangle, |0, 0\rangle|n\rangle\}_{n=2}^\infty, \end{aligned} \quad (3)$$

with blocks given by the following matrices

$$\begin{aligned} H^{(0)} &= 0, \quad H^{(1)} = \hbar g \begin{pmatrix} 0 & \sqrt{2} \\ \sqrt{2} & 0 \end{pmatrix}, \\ H^{(n \geq 2)} &= \hbar g \begin{pmatrix} 0 & \sqrt{2(n-1)} & 0 \\ \sqrt{2(n-1)} & 0 & \sqrt{2n} \\ 0 & \sqrt{2n} & 0 \end{pmatrix}. \end{aligned} \quad (4)$$

The eigenvalues of these matrices are given by  $\{0\}$  for  $n = 0$ ,  $\{-\sqrt{2}\hbar g, \sqrt{2}\hbar g\}$  for  $n = 1$ , and  $\{0, -\hbar\omega_n, \hbar\omega_n\}$  for  $n \geq 2$ , with

$$\omega_n = g\sqrt{4n-2}. \quad (5)$$

The transformations that diagonalize each of the blocks  $H^{(n)}$  are given by

$$\begin{aligned} O^{(1)} &= \frac{1}{\sqrt{2}} \begin{pmatrix} 1 & 1 \\ -1 & 1 \end{pmatrix}, \\ O^{(n \geq 2)} &= \frac{1}{\sqrt{4n-2}} \begin{pmatrix} -\sqrt{2n} & \sqrt{n-1} & \sqrt{n-1} \\ 0 & -\sqrt{2n-1} & \sqrt{2n-1} \\ \sqrt{2n-2} & \sqrt{n} & \sqrt{n} \end{pmatrix}. \end{aligned} \quad (6)$$

These matrices are the blocks of the orthogonal transformation  $\hat{O}$  that diagonalizes the Hamiltonian  $\hat{H}$  as  $\hat{O}^\dagger \hat{H} \hat{O}$ .

### A. Exact solution

Having solved the eigenvalue problem for  $\hat{H}$ , it is now possible to evaluate the time-dependent state vector

$$|\Psi_t\rangle = e^{-i\hat{H}t/\hbar} |\Psi_0\rangle \quad (7)$$

for any given initial pure state  $|\Psi_0\rangle$ . In this work we consider as initial condition a normalized product state of the two atoms and the single-mode field that can be expressed as

$$\begin{aligned} |\Psi_0\rangle &= |\Psi_0^{\text{at}}\rangle |\alpha\rangle, \\ |\Psi_0^{\text{at}}\rangle &= c_0 |0, 0\rangle + c_- |\Psi^-\rangle + c_+ |\Psi^+\rangle + c_1 |1, 1\rangle. \end{aligned} \quad (8)$$

We have considered a general pure state  $|\Psi_0^{\text{at}}\rangle$  of the atoms with probability amplitudes  $c_\pm$ ,  $c_0$  and  $c_1$ . For the single mode of the radiation field we have chosen a coherent state

$$|\alpha\rangle = \sum_{n=0}^\infty e^{-\frac{|\alpha|^2}{2}} \frac{\alpha^n}{\sqrt{n!}} |n\rangle, \quad \alpha = \sqrt{\bar{n}} e^{i\phi}, \quad (9)$$

with mean photon number  $\bar{n}$ . Using the eigenbasis of  $\hat{H}$ , the exact solution of the time-dependent state vector can be written as

$$|\Psi_t\rangle = |0, 0\rangle |\chi_t^{-1}\rangle + |\Psi^+\rangle |\chi_t^0\rangle + |1, 1\rangle |\chi_t^1\rangle + c_- |\Psi^-\rangle |\alpha\rangle \quad (10)$$

with the relevant photonic states

$$\begin{aligned} |\chi_t^{-1}\rangle &= c_0 p_0 |0\rangle + \sum_{n=1}^{\infty} \frac{\sqrt{n} (\xi_{n,t}^- - \xi_{n,t}^+) + \sqrt{n-1} \xi_n}{\sqrt{2n-1}} |n\rangle, \\ |\chi_t^0\rangle &= \sum_{n=1}^{\infty} (\xi_{n,t}^- + \xi_{n,t}^+) |n-1\rangle, \\ |\chi_t^1\rangle &= \sum_{n=2}^{\infty} \frac{\sqrt{n-1} (\xi_{n,t}^- - \xi_{n,t}^+) - \sqrt{n} \xi_n}{\sqrt{2n-1}} |n-2\rangle, \end{aligned} \quad (11)$$

and with the aid of the following abbreviations

$$\begin{aligned} \xi_{n,t}^{\pm} &= \frac{e^{\pm i\omega_n t}}{2} \left( c_{\pm} \mp \frac{c_0 p_n + \sqrt{n-1} c_1 p_{n-2}}{\sqrt{2n-1}} \right), \\ \xi_n &= \frac{\sqrt{n-1} c_0 p_n - \sqrt{n} c_1 p_{n-2}}{\sqrt{2n-1}}, \quad p_n = \alpha^n \sqrt{e^{-|\alpha|^2}/n!}. \end{aligned} \quad (12)$$

### B. Coherent-state approximation

The time-dependent solution of the state vector can be significantly simplified in the case of high values of the mean photon number, i.e.,  $\bar{n} \gg 1$ . In this limit  $\bar{n} \gg \sqrt{\bar{n}}$ , i.e., the mean of the Poisson distribution  $\bar{n}$  is much larger than the standard deviation  $\sqrt{\bar{n}}$ . Therefore we approximate  $\sqrt{(n-1)/(2n-1)}$  and  $\sqrt{n/(2n-1)}$  by  $1/\sqrt{2}$  and we also use the approximations

$$\begin{aligned} p_n &= \sqrt{\frac{\bar{n}}{n}} e^{i\phi} p_{n-1} \approx e^{i\phi} p_{n-1}, \\ \omega_n/g &\approx \sqrt{4\bar{n}+2} + 2 \frac{n - \bar{n} - 1}{\sqrt{4\bar{n}+2}}. \end{aligned} \quad (13)$$

The last line is obtained from the first-order Taylor expansion in  $n$  of the frequencies around  $\bar{n}+1$ . This is valid whenever the product between the second-order contribution times the interaction time  $t$  remains small, a condition that is satisfied when  $gt \ll \bar{n}$  [18, 19]. With these considerations and by introducing the abbreviations

$$\eta_{\pm} = \frac{1}{2} (c_{\pm} \mp d_{\phi}^{\pm}), \quad d_{\phi}^{\pm} = \frac{e^{i\phi} c_0 \pm e^{-i\phi} c_1}{\sqrt{2}}, \quad (14)$$

the photonic states can be simplified to

$$\begin{aligned} |\chi_t^k\rangle &\approx \frac{e^{ik\phi}}{\sqrt{1+|k|}} \left( \eta_- |F_{k,t}^- \rangle + (-1)^k \eta_+ |F_{k,t}^+ \rangle - k d_{\phi}^- |\alpha\rangle \right), \\ k &\in \{-1, 0, 1\}, \end{aligned} \quad (15)$$

where we have introduced the field states

$$|F_{k,t}^{\pm}\rangle = e^{\pm i2gt \frac{1+k(\bar{n}+1)}{\sqrt{4\bar{n}+1}}} |\alpha e^{\frac{\pm i2gt}{\sqrt{4\bar{n}+1}}}\rangle, \quad k \in \{-1, 0, 1\}. \quad (16)$$

which are coherent states up to an additional phase.

### C. Atomic postselection

The description in terms of coherent states allows a simpler analysis of the dynamics. Our aim is to prepare the atoms in an atomic postselection scenario where the atoms are prepared conditioned to a successful projection of the field onto the initial coherent state  $|\alpha\rangle$  in a simplified and ideal implementation. In such a case, one would have to consider the following overlaps

$$\langle \alpha | \chi_t^k \rangle \approx -k e^{ik\phi} \frac{e^{i\phi} c_0 \pm e^{-i\phi} c_1}{2}. \quad (17)$$

This result can be obtained by noting that the overlap between coherent states is given by

$$\left| \langle \alpha | \alpha e^{\frac{\pm i2gt}{\sqrt{4\bar{n}+1}}} \rangle \right| = \left| \exp \left[ -\bar{n} \left( 1 - e^{\frac{\pm i2gt}{\sqrt{4\bar{n}+1}}} \right) \right] \right| \approx e^{-g^2 t^2},$$

which can be neglected if  $gt \gg 1$ . Therefore, after interaction with the resonator and projection onto state  $|\alpha\rangle$ , both atoms are left in the state

$$\frac{c_-}{Q_1} |\Psi^- \rangle + \frac{e^{i\phi} c_0 - e^{-i\phi} c_1}{2Q_1} (e^{-i\phi} |0, 0\rangle - e^{i\phi} |1, 1\rangle), \quad (18)$$

with  $Q_1^2 = |c_1|^2 + |e^{i\phi} c_0 - e^{-i\phi} c_1|^2/2$  success probability. The final state is actually a superposition of two states with probability amplitudes proportional to the initial ones. Therefore, the atomic postselection can be understood as a projection of the atomic state with the following rank two projector

$$\hat{M} = |\Psi^- \rangle \langle \Psi^-| + |\Phi_{\phi}^- \rangle \langle \Phi_{\phi}^-|, \quad (19)$$

where we have introduced the state  $|\Phi_{\phi}^- \rangle = (e^{-i\phi} |0, 0\rangle - e^{i\phi} |1, 1\rangle) / \sqrt{2}$ . The operation  $\hat{M}$  represents the effective description of the interaction of the atoms with the resonator and the postselection via measurement of the field.

### D. Atomic postselection by balanced homodyne detection

Considering the projection onto a coherent state is an idealization that provides a convenient simplified picture. In practice, however, it is sufficient to project onto a state with vanishing overlap with the time-dependent field components  $|F_{k,t}^{\pm}\rangle$  and with finite overlap with  $|\alpha\rangle$ . A typical experimental setting able to achieve this goal is a balanced homodyne measurement [18]. The basic idea is to use a 50/50 beam splitter to combine the field to be measured with a reference coherent field parametrized by its phase  $\theta$ . Photons from the two outputs of the beam splitter are collected using photodetectors. In the strong limit of the reference field [20], the probability of measuring a photocurrent difference between the detectors is proportional to the projection of the field onto the eigenstate  $|q_{\theta}\rangle$  of a field quadrature  $\hat{q}_{\theta} = (\hat{a}e^{-i\theta} + \hat{a}^{\dagger}e^{i\theta})/\sqrt{2}$ .

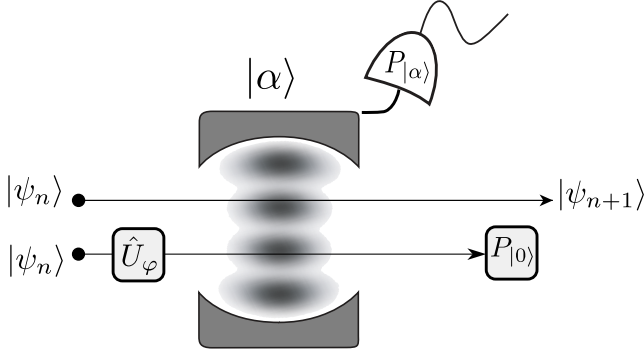


FIG. 1: Two two-level atoms in the same state  $|\psi_n\rangle$  interact with an optical resonator prepared in a coherent state  $|\alpha\rangle$ . Before the interaction, the gate  $\hat{\sigma}_z$  is applied to one of the atoms and after the interaction this same atom is projected onto its ground state. The field is projected onto the initial coherent state. Finally one of the atoms is left in the state  $|\psi_{n+1}\rangle$ .

This probability density for a coherent state  $|\alpha\rangle$  is given by

$$|\langle q_\theta|\alpha\rangle|^2 = \frac{1}{\sqrt{\pi}} \exp\{-[q_\theta - \tilde{q}_\theta]^2\} \quad (20)$$

with  $\tilde{q}_\theta = (\alpha e^{-i\theta} + \alpha^* e^{i\theta})/\sqrt{2}$ . This can attain values close to unity by choosing the phase in such a way that  $\tilde{q}_\theta = 0$  and restricting values of  $q_\theta$  close to zero. The square of the overlap with the other field components, that are also coherent states, can be evaluated as

$$|\langle q_\theta|F_{kmt}^\pm\rangle|^2 = \frac{1}{\sqrt{\pi}} \exp\{-[q_\theta - \tilde{q}_{\Theta_t^\pm}]^2\}, \quad (21)$$

with  $\Theta_t^\pm = \theta \mp 2gt/\sqrt{4\tilde{n}+1}$ . By choosing an appropriate interaction time  $t$ , these overlaps can be made exponentially small.

### III. A NONLINEAR MAP OF PURE ATOMIC STATES

In this section we use the atomic postselection scheme of the two-atom Tavis-Cummings model in order to implement an entangling quantum operation which by iteration leads to a nonlinear mapping of atomic probability amplitudes. The protocol is depicted schematically in Fig. 1. We consider the two two-level atoms initially prepared in a product state of the form ( $z \in \mathbb{C}$ )

$$|\Psi_0^{\text{at}}\rangle = |\psi_0\rangle_A \otimes |\psi_0\rangle_B, \quad |\psi_0\rangle = \frac{|0\rangle + ze^{i\phi}|1\rangle}{\sqrt{1+|z|^2}}. \quad (22)$$

For later convenience we have included the phase  $\phi$  of the coherent state. Before interacting with the optical resonator, a unitary gate  $\hat{U}_\varphi^B$  is applied to atom  $B$ . We

choose the following gate

$$\hat{U}_\varphi = \begin{pmatrix} e^{i\varphi} & 0 \\ 0 & -e^{-i\varphi} \end{pmatrix}, \quad (23)$$

which can be implemented by driving the atom with a resonant electromagnetic field and properly controlling the coupling and duration of the interaction [21, 22]. After the application of  $\hat{U}_\varphi^B$  and before entering the resonator we get the following atomic probability amplitudes

$$\begin{aligned} c_0 &= \langle 0, 0 | \hat{U}_\varphi^B | \Psi_0^{\text{at}} \rangle = -e^{-i\varphi}/(1+|z|^2) \\ c_1 &= \langle 1, 1 | \hat{U}_\varphi^B | \Psi_0^{\text{at}} \rangle = z^2 e^{-i2\varphi}/(1+|z|^2) \\ c_- &= \langle \Psi^- | \hat{U}_\varphi^B | \Psi_0^{\text{at}} \rangle = \sqrt{2} z e^{i\phi} \cos \varphi / (1+|z|^2). \end{aligned} \quad (24)$$

The probability amplitude  $c_+$  does not need to be specified, as the resulting quantum operation projects the atoms onto a subspace orthogonal to  $|\Psi^+\rangle$  as can be noted from Eq. (18). With these initial conditions, both atoms interact with the electromagnetic field inside an optical cavity prepared in a coherent state  $|\alpha\rangle$ . After the interaction a projection  $P_{|\alpha\rangle}$  of the field onto the initial coherent state  $|\alpha\rangle$  is performed and the atoms are left in the state

$$\frac{\sqrt{2} z e^{i\phi} \cos \varphi}{(1+|z|^2)Q_1} |\Psi^- \rangle - \frac{e^{-i\varphi} + z^2 e^{i\varphi}}{2(1+|z|^2)Q_1} (|0, 0\rangle - e^{i2\phi}|1, 1\rangle).$$

The success probability of this projection is

$$Q_1^2 = \frac{1+|z|^4 + 4|z|^2 \cos^2 \varphi + (z^2 e^{i\varphi} + \text{c.c.})}{2(1+|z|^2)^2}. \quad (25)$$

Afterwards a projection  $P_{|0\rangle}$  onto the ground state of atom  $B$  is implemented leaving atom  $A$  in the state

$$-\frac{ze^{i\phi} \cos \varphi}{(1+|z|^2)Q_1 Q_2} |1\rangle - \frac{e^{-i\varphi} + z^2 e^{i\varphi}}{2(1+|z|^2)Q_1 Q_2} |0\rangle. \quad (26)$$

This event occurs with success probability  $Q_2 = 1/2$ . The overall success probability of the postselections is then given by

$$P_s = Q_2^2 Q_1^2 = Q_1^2/2 \geq \frac{\cos^2 \varphi}{4}. \quad (27)$$

The last inequality follows from analyzing Eq. (25) and noting that  $Q_1$  attains its minimum value when  $|z|^2 = 1$  and  $\text{Re}[z^2 e^{i\varphi}] = -1$ . Up to normalization the final state is given by

$$|0\rangle + \frac{2z \cos \varphi}{e^{-i\varphi} + z^2 e^{i\varphi}} e^{i\phi} |1\rangle. \quad (28)$$

By iterating this procedure we attain a scheme implementing the following quantum map for the  $(n+1)$ th step

$$\frac{|0\rangle + f_\varphi^n(z) e^{i\phi} |1\rangle}{\sqrt{1+|f_\varphi^n(z)|^2}} \rightarrow \frac{|0\rangle + f_\varphi^{n+1}(z) e^{i\phi} |1\rangle}{\sqrt{1+|f_\varphi^{n+1}(z)|^2}} \quad (29)$$

with the complex functions

$$f_\varphi(z) = \frac{2z \cos \varphi}{e^{-i\varphi} + z^2 e^{i\varphi}},$$

$$f_\varphi^{n+1}(z) = f_\varphi(f_\varphi^n(z)), \quad f_\varphi^0(z) = z. \quad (30)$$

The map is independent of the parameter  $\phi$ , as one can note that the phase factor  $e^{i\phi}$  appears in the probability amplitude of state  $|1\rangle$  in the same manner as in the initial state  $|\psi_0\rangle$  of Eq. (22).

We note that the iteration of the map involves repeated action of the protocol on an ensemble of atoms. The protocol acts on a pair of identically prepared atoms from the ensemble and prepares one atom probabilistically. The other atom becomes useless from the point of view of the protocol, as a result of the projective measurement on it. After acting on all the atoms of the ensemble, one arrives at a smaller ensemble of less than one half in size. Rapid downscaling of the ensemble size is a unavoidable condition for any quantum dynamics truly sensitive to initial conditions [11]. In practice, realizing many steps of the protocol would require an exponentially large initial ensemble which would not be realistic. Another practical aspect is that employing more than one cavity would be challenging with today's experimental possibilities. On the other hand, as we will demonstrate in the next sections, already a few steps can be enough to make highly overlapping initial quantum states almost orthogonal. Furthermore we will outline an experimental proposal in Sec. VI with currently available technology by applying an optical conveyor belt and a single cavity.

#### IV. BASIC PROPERTIES OF THE NONLINEAR MAP

The dynamics within the approximations we have made is fully described by the iterative complex function in Eq. (30). This is a quadratic rational map [25], similar to the maps occurring in the measurement induced nonlinear quantum dynamical schemes first described in [3, 4, 11]. In the following, we first carry out an analysis of the general properties of the iterated map  $f_\varphi$  of Eq. (30) by using concepts from the theory of complex dynamical maps [26]. Then we compare its behavior to the numerical solution of the complete iterated dynamics, based on the Hamiltonian of Eq. (1) and the subsequent selective measurements.

##### A. Stable cycles

The periodic orbits or fixed cycles of the map  $f_\varphi$  can be determined from the relation  $f_\varphi^n(z) = z$ . The one-cycles or fixed points as well as the 2-cycles can be determined analytically. For  $n = 1$  we find

$$z_j^{(1)} = j, \quad j \in \{-1, 0, 1\}. \quad (31)$$

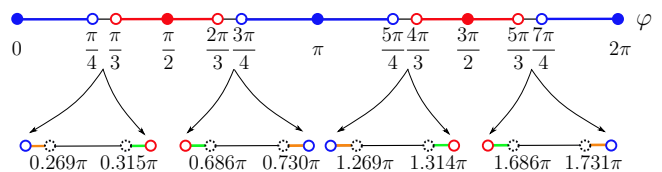


FIG. 2: Stability of the fixed cycles of  $f_\varphi$  as a function the parameter  $\varphi$ . Blue corresponds to the one-cycles  $z^{(1)} = \pm 1$ , red corresponds to  $z^{(1)} = 0$ . Dots, lines, and circles represent superattractive, attractive, and neutral cycles, respectively. Numerical investigation of the enlarged regions between the neutral one-cycles show two different attractive 4-cycles (orange lines) and a single attractive 6-cycle (green lines) close to the two ends of the region. The central part of the enlarged regions contain "islands" of attractive  $n \geq 60$  cycles. The dotted circles indicate that is hard to identify the border of different regions.

For  $n = 2$ , in addition to the above one-cycles, one can find two more points which are transformed into each other by  $f_\varphi$ . These form the single nontrivial two-cycle

$$z_k^{(2)} = (-1)^k i \sqrt{1 + 2e^{-2i\varphi}}, \quad k \in \{1, 2\}. \quad (32)$$

The stability of the fixed cycles can be checked by calculating the multiplier  $\lambda = (f_\varphi^n)'(z_j) = f_\varphi'(z_1)f_\varphi'(z_2)\dots f_\varphi'(z_n)$ . A fixed cycle is repelling, neutral, attractive, or superattractive if  $|\lambda| > 1$ ,  $|\lambda| = 1$ ,  $|\lambda| < 1$ , or  $|\lambda| = 0$ , respectively. Such an analysis can be carried out analytically for the one- and two-cycles, however, for  $n \geq 2$  it is a nontrivial task. The analysis of the multipliers shows that for each of the one-cycles there are certain parameter regions where they are attractive. On the other hand, the two-cycle given by Eq. (32), is repelling for any value of  $\varphi$ .

For the determination of the longer ( $n \geq 3$ ) attractive cycles we can use the method based on the iteration of the critical points of the map. The critical points of  $f_\varphi$  are those which solve the equation  $f_\varphi'(z) = 0$ . In this case, there are two critical points:

$$z_{c\pm} = \pm e^{-i\varphi}. \quad (33)$$

A general theorem on iterated rational polynomial maps states that a rational map of degree  $d$  can have at most  $2d-2$  attractive cycles. Following the orbits of the critical points one can find all stable cycles of the iterated map (in this case at most 2).

Fig. 2 shows where, according to the analytical calculations, the one-cycles are superattractive (dots), attractive (lines), and neutral (circles) as a function of the parameter  $\varphi$ . The numerical iteration of the critical points in the regions between the neutral one-cycles shows that there are two different attractive 4-cycles (orange lines) and a single 6-cycle (green lines) close to the two ends of the regions. The actual  $z$  values belonging to the attractive 4- and 6-cycles depend on the parameter  $\varphi$ . In between these regions, it is numerically hard to rule out the existence of very long stable periodic orbits. The precision

of our numerical simulation made it possible to identify a few "islands" of attractive fixed cycles of  $n \geq 60$ . The remaining part of this region may belong to maps without any stable periodic orbit, which means that all initial states belong to the Julia set. The dotted circles indicate that the border between different regions is hard to determine numerically, which is an indication of the fractal nature of the regions. Let us note that for  $\varphi = \pi/2$  and  $3\pi/2$  the map is actually not a genuine complex map since  $f_\varphi \equiv 0$  in these cases.

### B. Nature of the iterated map

The fractal nature of the map is more apparent when one determines the Julia set of  $f_\varphi$ , i.e. the set of points which do not converge to an attractive cycle for a given  $\varphi$ . One way of numerically finding the points belonging to the Julia set is backwards iterating the map starting from a point which is an element of a repelling cycle of the map. We show in Fig. 3 the Julia set of  $f_\varphi$  for  $\varphi = 1.666\pi$ . In this case, the Julia set is a totally disconnected set, all other initial points converge to the single attractive cycle  $z = 0$ , or physically speaking to the state  $|0\rangle$ . The analysis of the orbits of the critical points reveals important properties of the Julia set. In this case both critical points converge to the same attractive fixed point, consequently the Julia set is totally disconnected, similarly to the well-known Cantor set [25]. Another important case

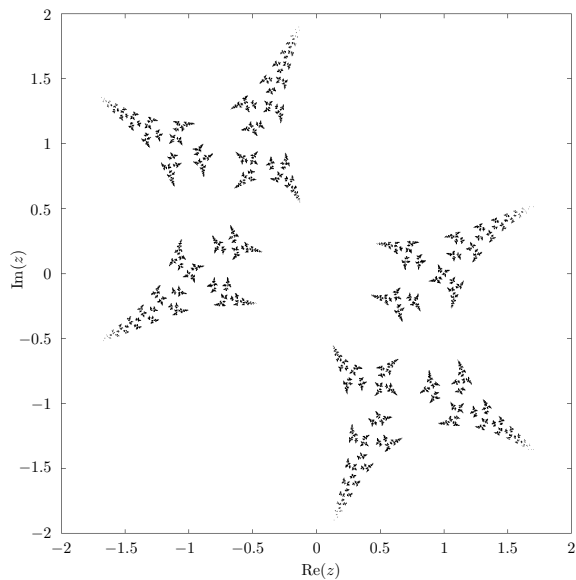


FIG. 3: The Julia set of the map  $f_\varphi$  for  $\varphi = 1.666\pi$ .

is when the two critical points converge to two distinct fixed points, then the Julia set is connected. This case is illustrated by the map at parameter value  $\varphi = 0.95\pi/4$  shown in Fig. 4. For quadratic rational maps a general theorem ensures that the Julia set is either totally disconnected, or connected [26].

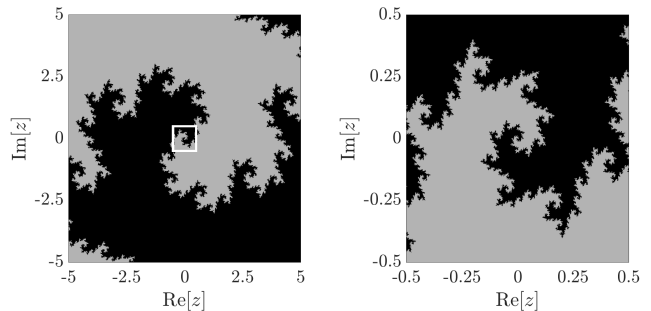


FIG. 4: Complex plane after 97 iterations of the map in Eq. (29) for  $\varphi = 0.95\pi/4$ . Two amplification levels are shown, confirming the fractal structure of the Julia set separating the regions whose points converge to the attractive fixed points 1 (grey) and  $-1$  (black). The region indicated by the square in the middle of the left figure is magnified in the right figure.

### C. Iteration of the complete dynamics

In order to investigate the real performance of the two-atom Tavis-Cummings model without the approximations of Sec. II, we compute a numerically exact version of the operator  $\hat{M}$  in Eq. (19). The matrix elements are evaluated as

$$M_{j,k} = \langle \alpha | \langle e_j | e^{-i\hat{H}t/\hbar} | e_k \rangle | \alpha \rangle \quad (34)$$

where we considered the atomic basis  $|e_j\rangle \in \{|1,1\rangle, |1,0\rangle, |0,1\rangle, |0,0\rangle\}$ . The interaction time  $t$  and coupling strength  $g$  satisfy the relation  $gt = \pi\sqrt{\bar{n}}/2$ . Each iteration of the map is then evaluated by renormalizing the following outcome  $\langle 0 |_B \hat{M} \hat{U}_B | \Psi_0^{\text{at}} \rangle$  for qubit A. In Fig. 5 we plotted the real part of the 97th iteration for two different values of the mean photon number  $\bar{n}$ , namely 100, and 10. With precision of two (one) decimal places the two fixed points also converge to  $+1$  and  $-1$  in the case of  $\bar{n} = 100$  ( $\bar{n} = 10$ ). Both figures reveal a fractal structure which resembles more the ideal case for larger values of  $\bar{n}$ .

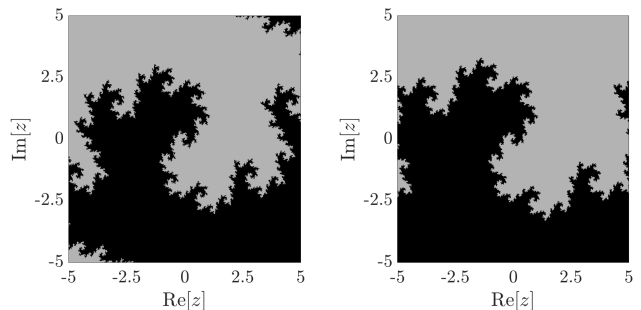


FIG. 5: The same as left part of Fig. 4 for the numerically exact quantum map and two values of the mean photon number  $\bar{n}$ : 100 (left) and 10 (right).

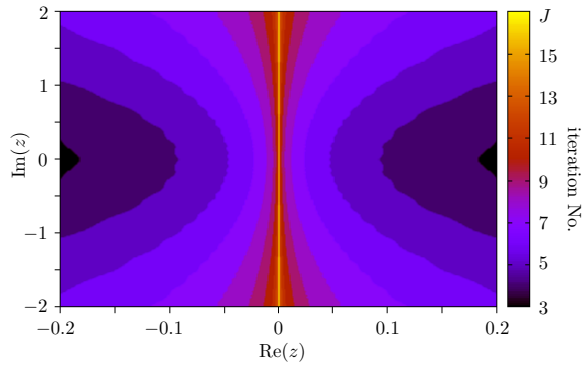


FIG. 6: The plane of initial states colored according to the number of iterations needed for a complex number  $z$  to reach either of the fix points 1 or  $-1$  with a precision of 0.1.

### V. AN APPLICATION FOR STATE DISCRIMINATION: THE SCHRÖDINGER MICROSCOPE

The number of atoms needed grows exponentially with the number of iterations even in an ideal case, which follows from the quantum magnification bound [11]. In a realistic experiment, one can expect that only a few steps of the iteration can be carried out. We propose a test here, which would demonstrate the strong nonlinear behavior of the evolution even after 2 or 3 steps. A useful aspect of nonlinear quantum state transformations is that small initial differences between two similar quantum states can be amplified, enabling to distinguish them, realizing a Schrödinger microscope, a term originally suggested by Lloyd and Slotine [10].

Let us consider the simple case when  $\phi = 0$ . In this case the unitary of Eq. (23) will become the well-known Z gate. We choose two initial quantum states close to each other in the form of Eq. (22) with  $z_1 = -0.2$ , and  $z_2 = 0.2$ . Their overlap is close to unity,  $|\langle\psi_1|\psi_2\rangle| \sim 0.92$ . The two states will become almost orthogonal (with a scalar product of  $\sim 0.08$ ) after three steps of the iteration as can be seen in Fig. 6 where we show the plane of initial states colored according to the number of iterations needed for a complex number  $z$  to reach either of the fix points 1 or  $-1$  with a precision of 0.1. The Julia set of the map is indicated by the yellow region on the figure, coinciding with the imaginary axis.

In Fig. 7 we show the evolution of the overlap of the above two initial states using the complete solution with mean photon numbers  $\bar{n} = 10$  and  $\bar{n} = 100$  and by using the idealized map (30). Interestingly, the low-photon-number case leads to a faster decrease in the overlap during the first few steps of the iteration, but then converges to a larger value compared to the ideal map.

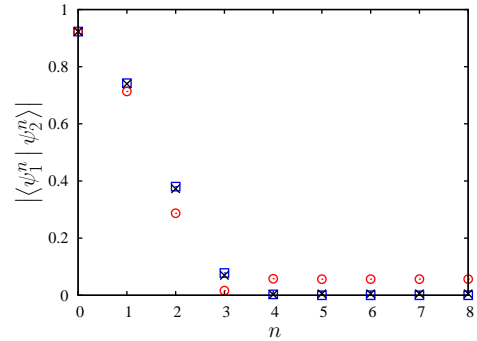


FIG. 7: The overlap of the states  $|\psi_1\rangle = 0.98(|0\rangle - 0.2|1\rangle)$  and  $|\psi_2\rangle = 0.98(|0\rangle + 0.2|1\rangle)$  after  $n$  iterations of the ideal map (blue squares), and the complete map with mean photon number 10 (red circles) and 100 (black crosses).

### VI. EXPERIMENTAL CONSIDERATIONS

Our basic protocol involves atomic and photonic post-selection and therefore there is always a finite probability of failure. This means that in order to implement several iterations of the map, one requires several copies of the initial qubit pair. The procedure explained in Sec. III has to be applied to every single copy of the ensemble. The number  $N$  of qubit pairs required to achieve  $n$  iterations, can be bounded from below by taking into account the success probability  $P_s$  in (27). In addition, one has to take into account that half of the atoms in the ensemble are lost after being measured. Therefore, the number of pairs scales exponentially as  $N = (2/P_s)^n = (8/\cos^2\varphi)^n$ .

On a first thought one would naively consider the use of  $N$  optical cavities for  $N$  atomic pairs. However, there is another simpler solution motivated by current experimental implementations [23, 24], where a standing-wave dipole trap or “optical conveyor belt” is used to coherently transport neutral atoms into an optical resonator.

Using this setting, two conveyor belts are required to transport atoms into the cavity. In an initial stage,  $N$  atoms are prepared in the minima of the two optical traps and are aligned as depicted in Fig. 8. For convenience, we number the atoms from left to right. The unitary gate  $\hat{U}_\varphi$  is applied at this preparatory stage to atoms labeled with an even (odd) number in the upper (lower) conveyor belt, we call them marked atoms. The two conveyor belts are moved forward into the direction of the cavity until the first pair reaches the other side of the cavity. Then, the conveyor belts stop in order to allow the measurement of the first marked atom and the field inside the cavity. Afterwards, the cavity is reset to the state  $|\alpha\rangle$  and the conveyor belts move again repeating the process. After all atoms have interacted with the cavity, the marked atoms are blacklisted as they are no longer useful. They are depicted in gray in Fig. 8. In order to pair only the useful atoms, the lower conveyor belt is shifted one period to the left, leaving the first marked atom without a partner. In this way, the



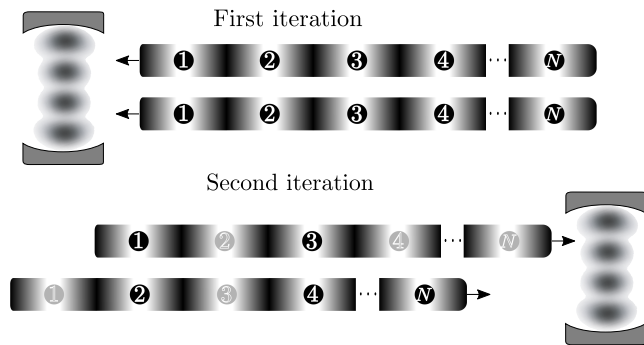


FIG. 8: Possible implementation of the protocol using neutral atoms coherently transported using optical conveyor belts.

potentially successfully prepared atoms are aligned. The process is repeated with both conveyor belts moving to the opposite side to start the second iteration. In the aforementioned implementation of the second iteration we have ignored the possibility of failure in the postselection. In order to overcome this problem, one has to keep track of successfully prepared atoms and then shift the conveyor belts in order to align useful pairs before transporting them into the cavity.

## VII. CONCLUSION

We have proposed a non-linear map of qubit states in a cavity quantum electrodynamical scenario where the qubits are encoded in two-level atoms. The core step requires the interaction of two equally prepared atoms with the field inside an optical resonator according to the Tavis-Cummings model. By subsequent field detection and selective measurement of one of the atoms, the unmeasured atom is postselected into a state nonlinearly depending on its initial state.

From a mathematical point of view, we have studied the complex function describing this mapping of pure qubit states, where we have exploited the fact that any

pure state of a qubit can be described by a complex parameter. We have performed an analysis of stable cycles under the iteration of the function and studied the behaviour in the complex plane. In particular, we have numerically investigated the Julia set which changes from connected to disconnected for different parameters of the system. Thus, our study offers a demonstration of chaotic behaviour in a quantum mechanical setting involving sequences of unitary transformations and post-selective measurements.

From a physical perspective, we have proposed the realization of this scheme using an ensemble of equally prepared atoms in two optical conveyor belts that are coherently transported and interact in pairs with a single optical resonator. We have estimated the number of atoms required for each iteration of the protocol taking into account the success probability of the measurements involved. As an application we have discussed a Schrödinger microscope implementation in which two initially close pure quantum states can be discriminated almost perfectly by a few iterations of our scheme.

Although possible realizations of this nonlinear qubit map require cutting edge quantum technological developments, such as optical conveyor belts and controlled two-qubit interactions with a single mode radiation field, in view of the rapid experimental advances in cavity quantum electrodynamics its realization is within reach of nowadays technology.

## Acknowledgments

This work was supported by the Hungarian Academy of Sciences (Lendület Program, LP2011-016) and the National Research, Development and Innovation Office (K115624, NN109651) and by the Deutscher Akademischer Austauschdienst (MÖB-DAAD project no. 65049). O. K. acknowledges support from the János Bolyai Research Scholarship of the Hungarian Academy of Sciences.

- 
- [1] F. Haake, *Quantum Signatures of Chaos* (Springer, 2010).
  - [2] S. Habib, K. Jacobs and K. Shizume, Phys. Rev. Lett. **96**, 010403 (2006).
  - [3] Bechmann-Pasquinucci, H., B. Huttner and N. Gisin, Phys. Lett. A **242**, 198 (1998).
  - [4] T. Kiss, I. Jex, G. Alber and S. Vymětal, Phys. Rev. A, **74**, 040301(R) (2006)
  - [5] C. H. Bennett, G. Brassard, S. Popescu, B. Schumacher, J. A. Smolin and W. K. Wootters, Phys. Rev. Lett. **76**, 722 (1996); **78**, 2031 (1997).
  - [6] D. Deutsch, A. Ekert, R. Jozsa, C. Macchiavello, S. Popescu and A. Sanpera, Phys. Rev. Lett. **77**, 2818 (1996); **80**, 2022 (1998).
  - [7] G. Alber, A. Delgado, N. Gisin and I. Jex, J. Phys. A **34**, 8821 (2001).
  - [8] C. Macchiavello, Phys. Lett. A **246**, 345 (1998).
  - [9] T. Kiss, S. Vymetal, L.D. Toth, A. Gabris, I. Jex and G. Alber, Phys. Rev. Lett. **107**, 100501 (2011).
  - [10] S. Lloyd and J.E. Slotin, Phys. Rev. A **62**, 012307 (2000).
  - [11] A. Gilyen, T. Kiss and I. Jex, Sci. Rep. **6**, 20076 (2016).
  - [12] S. Haroche, Rev. Mod. Phys. **85**, 1083 (2013).
  - [13] D. Wineland, Rev. Mod. Phys. **85**, 1103 (2013).
  - [14] Reimann, W. Alt, T. Kampschulte, T. Macha, L. Ratschbacher, N. Thau, S. Yoon and D. Meschede, Phys. Rev. Lett. **114**, 023601 (2015).
  - [15] A. Neuzner, M. Krber, O. Morin, S. Ritter and G.



- Rempe, Nat. Photonics **10**, 303 (2016).
- [16] D. Meschede, H. Walther and G. Muller, Phys. Rev. Lett. **54**, 551 (1985).
  - [17] M. Tavis and F. W. Cummings, Phys. Rev. **170**, 279 (1968).
  - [18] J.M. Torres, J.Z. Bernád and G. Alber, Phys. Rev. A **90**, 012304 (2014).
  - [19] J.M. Torres, J.Z. Bernád and G. Alber, Appl. Phys. B **122**, 117 (2016).
  - [20] A. I. Lvovsky and M. G. Raymer, Rev. Mod. Phys. **81**, 299 (2009).
  - [21] M. A. Nielsen and I. L. Chuang, *Quantum Computation and Quantum Information* (Cambridge University Press, Cambridge, UK, 2000).
  - [22] D. Meschede and A. Rauschenbeutel, Adv. At. Mol. Opt. Phys. **53**, 75 (2006).
  - [23] M. Khudaverdyan, W. Alt, I. Dotsenko, T. Kampschulte, K. Lenhard, A. Rauschenbeutel, S. Reick, K. Schrner, A. Widera and D. Meschede, New J. Phys., **10**, 073023 (2008).
  - [24] S. Brakhane, W. Alt, T. Kampschulte, M. Martinez-Dorantes, R. Reimann, S. Yoon, A. Widera and D. Meschede Phys. Rev. Lett., **109**, 173601 (2012).
  - [25] J. Milnor and Tan Lei, Experiment. Math. **2**, 37 (1993).
  - [26] J. Milnor, *Dynamics in One Complex Variable*, Annals of Mathematical Studies (Princeton University Press, 2006).